The Astrophysical Journal, 960:59 (8pp), 2024 January 1 https://doi.org/10.3847/1538-4357/ad054a

On the Formation and Interaction of Multiple Supermassive Stars in Cosmological Flows

Tyrone E. Woods[1,2], Samuel Patrick[3], Daniel J. Whalen[3], and Alexander Heger[4,5,6,7]
[1] National Research Council of Canada, Herzberg Astronomy and Astrophysics Research Centre, 5071 West Saanich Road, Victoria, BC V9E 2E7, Canada; tyrone.woods@umanitoba.ca
[2] Department of Physics and Astronomy, Allen Building, 30A Sifton Road, University of Manitoba, Winnipeg MB R3T 2N2, Canada
[3] Institute of Cosmology and Gravitation, University of Portsmouth, Portsmouth PO1 3FX, UK
[4] Monash Centre for Astrophysics, School of Physics and Astronomy, Monash University, VIC 3800, Australia
[5] ARC Centre of Excellence for Gravitational Wave Discovery (OzGrav), Melbourne, Australia
[6] ARC Centre of Excellence for Astrophysics in Three Dimensions (ASTRO-3D), Australia
[7] Joint Institute for Nuclear Astrophysics, 1 Cyclotron Laboratory, National Superconducting Cyclotron Laboratory, Michigan State University, East Lansing, MI 48824-1321, USA
Received 2021 December 13; revised 2023 October 12; accepted 2023 October 18; published 2023 December 22

Abstract

Supermassive primordial stars with masses exceeding $\sim 10^5\,M_\odot$ that form in atomically cooled halos are the leading candidates for the origin of high-redshift quasars at $z > 6$. Recent numerical simulations, however, find that multiple accretion disks can form within a halo, each of which can potentially host a supermassive star. We investigate the formation and evolution of secondary supermassive stars in atomically cooled halos, including strong variations in their accretion histories driven by gravitational interactions between their disks and those surrounding the primary supermassive stars in each halo. We find that all secondary disks produce long-lived supermassive stars under sustained rapid accretion. We also find, however, that the majority of secondary supermassive stars do undergo at least one protracted quiescent accretion phase, during which time they thermally relax and may become powerful sources of ionizing feedback. In many halos, the two satellite disks collide, suggesting that the two stars can come into close proximity. This may induce additional mass exchange between them, leading to a great diversity of possible outcomes. These range from coevolution as main-sequence stars to main sequence—black hole pairs and black hole—black hole mergers. We discuss the likely outcome for these binary interactions based on the evolutionary state of both supermassive stars at the end of our simulations, as well as prospects for their future detection by current and next-generation facilities.

Unified Astronomy Thesaurus concepts: Supermassive black holes (1663); Primordial galaxies (1293); Population III stars (1285)

1. Introduction

Nearly 300 quasars powered by supermassive black holes (BHs) have now been discovered at $z > 6$ (Bosman 2021), including nine at $z > 7$ (Mortlock et al. 2011; Wu et al. 2015; Bañados et al. 2018; Wang et al. 2021). A natural explanation for the seeds of these quasars are direct-collapse BHs (DCBHs), which arise as a result of the collapse of supermassive stars (SMSs) formed in atomically cooled halos at $z \gtrsim 20$ (Bromm & Loeb 2003; Lodato & Natarajan 2006; Wise et al. 2008; Regan & Haehnelt 2009; Latif et al. 2013). In this picture, a primordial halo grows to $\sim 10^7\,M_\odot$ without forming stars because, for example, it is immersed in strong Lyman–Werner (LW) UV fluxes (Dijkstra et al. 2008; Agarwal et al. 2012; Latif et al. 2014) or highly supersonic streaming motions of gas relative to dark matter (Tanaka & Li 2014; Hirano et al. 2017; Schauer et al. 2017), or it is dynamically heated by violent mergers (Yoshida et al. 2003; Fernandez et al. 2014; Wise et al. 2019; Regan et al. 2020). At this mass, virial temperatures reach $\sim 10^4$ K that activate line cooling in hydrogen, which in turn triggers rapid baryon collapse at initial rates of 0.1–1 $M_\odot\,\mathrm{yr}^{-1}$. Stellar evolution calculations indicate that such flows, if they persist, build up 10^4–$10^5\,M_\odot$ stars that later collapse to DCBHs (Hirano et al. 2014; Umeda et al. 2016; Woods et al. 2017; Haemmerlé et al. 2018b; Herrington et al. 2023; see Woods et al. 2019 and Maio et al. 2019 for recent reviews). However, it is now known that the highly supersonic turbulence in the rare, massive, low-shear halos needed to fuel the growth of the DCBH to $10^9\,M_\odot$ by $z \sim 7$ (Tenneti et al. 2018; Lupi et al. 2021; Valentini et al. 2021) can create DCBHs without the need for strong UV backgrounds, supersonic baryon streaming motions, or even atomic cooling (Latif et al. 2022b).

Cosmological simulations of the collapse of atomically cooled halos have been run either at extremely high resolutions that can follow flows down to protostellar radii but only for short times because of time step restrictions (e.g., Becerra et al. 2015; Ardaneh et al. 2018; Becerra et al. 2018; Luo et al. 2018) or for the longer times required to evolve the flows over many dynamical times but at the cost of resolving fragmentation deep in the accretion disk of the star (e.g., Chon et al. 2018; Regan & Downes 2018; Suazo et al. 2019; Latif et al. 2021). The first simulations to evolve atomically cooled flows for the entire life of an SMS were Latif et al. (2020), which revealed that some could form in binaries or small clusters. Most recently, Patrick et al. (2023, hereafter P23) followed the collapse of a variety of atomically cooled halos for 2–4 Myr and found that multiple accretion disks could form in them, each of which could harbor an SMS. These disks experienced multiple close encounters that gravitationally torqued gas into their centers, triggering brief bouts of massive accretion onto their respective stars. These stars thus interacted indirectly with one another via

encounters between their accretion disks. Although the simulations suggested a variety of final outcomes for these objects, they did not evolve the stars themselves (although see Nandal et al. 2023, for some initial efforts to evolve these lower-mass stars independently).

Recently, Woods et al. (2021, hereafter W21) modeled the growth of the stars in the primary disks in P23 and found that they collapse at final masses of $1.1 \times 10^5\,M_\odot$ to $1.9 \times 10^5\,M_\odot$. While W21 note the existence of secondary and in some cases tertiary or more disks in halos in P23, they do not follow the evolution of SMSs in those disks. Here we investigate the coevolution of SMSs in those satellite disks with the Kepler Lagrangian stellar evolution and hydrodynamics code to determine their properties and how gravitational interactions between the main disk and its satellites govern them. Our Kepler models use the time-dependent accretion rates from the cosmological simulations, and we follow the evolution of the SMSs until the satellites were subsumed into the primary disk or torn apart by tidal interactions with them.

In Section 2 we describe our stellar evolution models. The evolution of the stars is examined in Section 3. From the interaction histories of the disks and the formation and collapse times of the stars in them we determine whether they form SMS–SMS, SMS–DCBH, or binary DCBH systems and discuss possible consequences and observational signatures in Section 4, before concluding in Section 5.

2. Numerical Methods

2.1. ENZO

Accretion rates for the companion stars in our study were taken from cosmological simulations with the ENZO adaptive mesh refinement code by P23. These simulations resolved accretion at the centers of the disks on 0.01 pc scales with six-species primordial gas chemistry (H, He, e^-, H^+, He^+, and He^{2+}) to approximate very high LW backgrounds that ensured isothermal atomic cooling in the halos. The simulations included collisional ionization and excitation cooling by H and He, recombination cooling by H and He, bremsstrahlung cooling, and inverse Compton cooling by the cosmic microwave background (Bryan et al. 2014). The accretion rates were tabulated by computing mass fluxes through a 0.134 pc sphere at the center of each disk at 10 kyr intervals.

The eight halos in P23 were chosen to span a range of assembly histories and spin parameters and had masses of $\sim$(1–9) $\times 10^7\ M_\odot$ at collapse at redshifts $z = 13.9$–20.4. Resolution at the smallest scales on which fragmentation is known to occur in the disks had to be sacrificed in these simulations to follow their evolution for the times required for the stars to form, evolve, and collapse (e.g., Becerra et al. 2015, 2018). Our accretion rates therefore exclude these fragments, but they are expected to fall onto the protostar prior to the main sequence (MS; Inayoshi & Haiman 2014). We show accretion rates only for the largest of the satellite disks in each halo in Figure 1, not smaller ones that could undergo partial collapse but are short-lived because they collide with the main disk or are tidally disrupted by it.

2.2. KEPLER

We follow the evolution of the stars with KEPLER (Weaver et al. 1978; Woosley et al. 2002). KEPLER typically partitions each star into a few thousand zones, over which it solves the energy and angular momentum equations,

$$\frac{dv}{dt} = 4\pi r^2 \frac{\partial P}{\partial m_r} + \frac{4\pi}{r}\frac{\partial Q}{\partial m_r} - \frac{G_{\rm rel} m_r}{r^2} \quad (1)$$

$$\frac{du}{dt} = -4\pi P \frac{\partial}{\partial m_r}(vr^2) + 4\pi Q \frac{\partial}{\partial m_r}\left(\frac{v}{r}\right) - \frac{\partial L}{\partial m_r} + \epsilon, \quad (2)$$

where r is the radius, v is the velocity, P is the pressure, u is the internal energy per unit mass, ϵ is the local energy generation rate per unit mass, and L is the rate of energy flow through a shell of radius r. We include a first-order post-Newtonian correction to the gravitational constant, $G_{\rm rel}$,

$$G_{\rm rel} = G\left(1 + \frac{P}{\rho c^2} + \frac{4\pi P r^3}{m_r c^2}\right)\left(1 - \frac{2Gm_r}{rc^2}\right)^{-1}. \quad (3)$$

In Equation (1), Q in the viscous term is

$$Q = \frac{4}{3}\,\eta_\nu r^4 \frac{\partial}{\partial r}\left(\frac{v}{r}\right), \quad (4)$$

where η_ν is the dynamic viscosity defined in Weaver et al. (1978),

$$\eta_\nu = \eta_R + \frac{3}{4} l_1 \rho c_s + \frac{3}{4} l_2^2\ \max(0, -\nabla \cdot \mathbf{v}), \quad (5)$$

which includes both the real viscosity, η_R, and the artificial viscosity, which can be modified arbitrarily to dampen acoustic oscillations during quiescent phases of the evolution of a star. In this study, we take the standard values of $l_1 = 0.1\Delta r$ and $l_2 = 2\Delta r$, where Δr is the width of a grid zone. At each time step, Kepler initially attempts to make an arbitrarily large jump Δt before iterating to find the maximum time step permitted by preset restrictions on the change in radius, temperature, density, luminosity, or velocity between zones, allowing us to model long-lived, quiescent evolutionary phases and to follow the emergence of shocks or the onset of collapse on short timescales. The masses of the stars at collapse triggered by the post-Newtonian instability (Chandrasekhar 1964) in Kepler are consistent with analytic predictions (Haemmerlé 2021).

To close these equations, nuclear burning and energy generation are coupled to the hydrodynamics and solved with an adaptive network (Woosley et al. 2004), convection is treated in a time-dependent manner with heat transport following the Ledoux criterion (Weaver et al. 1978), and a Helmholtz-like equation of state is used that incorporates electron–positron pair production, relativistic and nonrelativistic degenerate and nondegenerate electrons, and radiation (Timmes & Swesty 2000). We neglect mass loss because wind and pulsational mass losses are expected to be negligible relative to the accretion rates in these stars (Baraffe et al. 2001; Vink et al. 2001; Hosokawa et al. 2013). For simplicity, we neglect rotation, although it could affect the stellar structure (Haemmerlé et al. 2018a).

As in previous studies (Hosokawa et al. 2013; Woods et al. 2017; Haemmerlé et al. 2018b; Woods et al. 2021), we initialize all models as 10 $M_\odot$, $n = 3$ polytropes with central densities $\rho_c = 10^{-3}$ g cm^{-3} and temperatures $T_c = 1.2 \times 10^6$ K, i.e., at the onset of deuterium burning. We treat accretion onto the star and the associated advection of entropy as described in Woosley et al. (2004) and Woods et al. (2017). The star is evolved until the onset of collapse, the end of the ENZO simulation, or the time

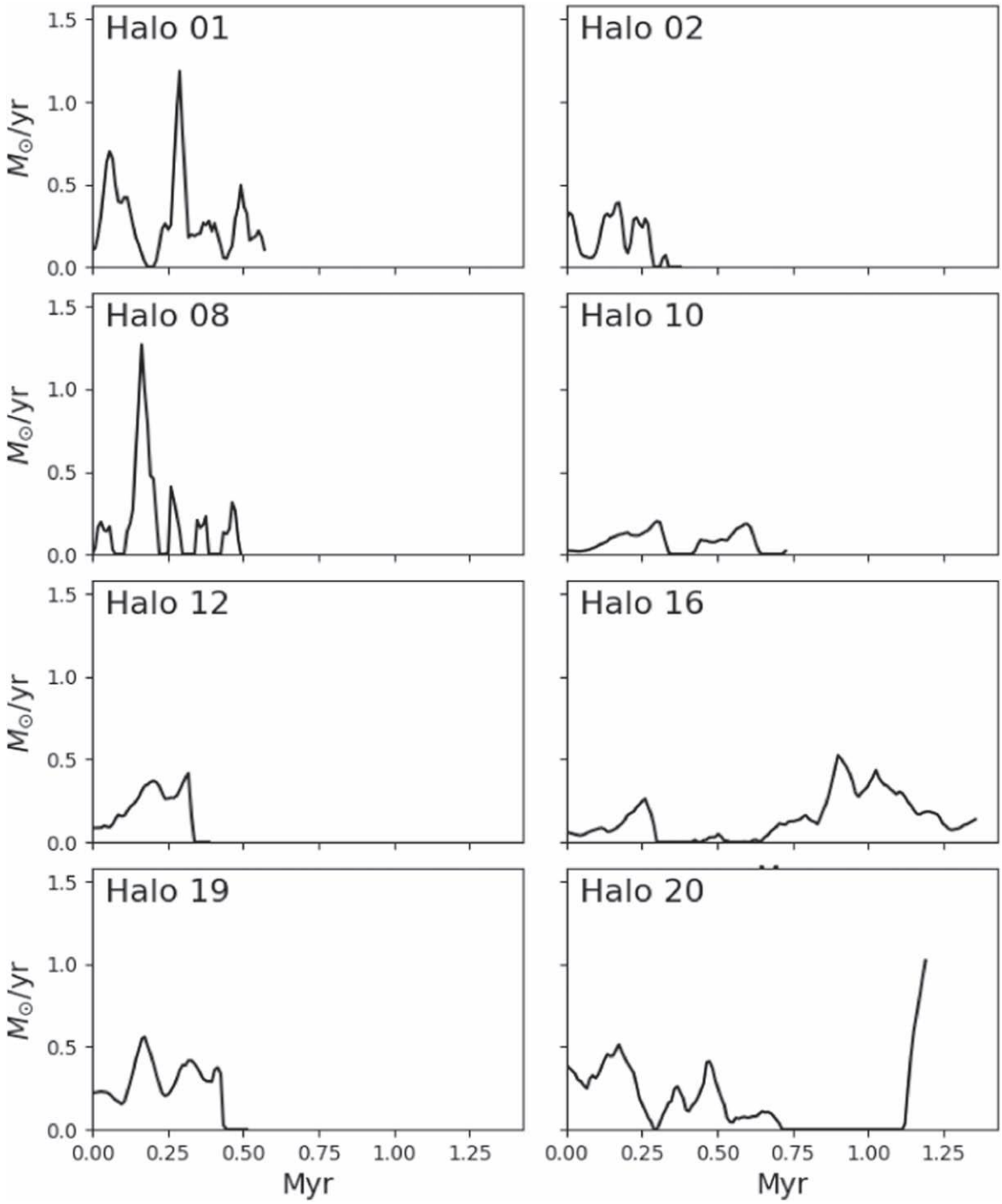

Figure 1. Accretion rates from P23 for the secondary stars. Note that times here are measured from the formation of the secondary disk, not the beginning of the simulation.

in the ENZO simulation when the companion disk merges with the primary disk.

3. Evolution of Multiple Supermassive Stars in Primordial Halos

3.1. Overall Features

We find that all the secondary disks form long-lived nuclear-burning stars. As with the stars in the primary disks in W21, we find a striking variety of internal structures for SMSs in the satellite disks as shown in Figure 2 (and with end states summarized in Table 1), in marked contrast to stars that evolve under constant accretion rates (e.g., Hosokawa et al. 2013; Woods et al. 2017; Haemmerlé et al. 2018b). They all initially have a deep radiative envelope that forms during the surge in accretion associated with the formation of their natal disks, which proceeds on much shorter times than the star's thermal timescale and leads to the buildup of a steep entropy gradient (e.g., Begelman 2010; Hosokawa et al. 2013; Woods et al. 2017; Haemmerlé et al. 2018b). In some models, we see the

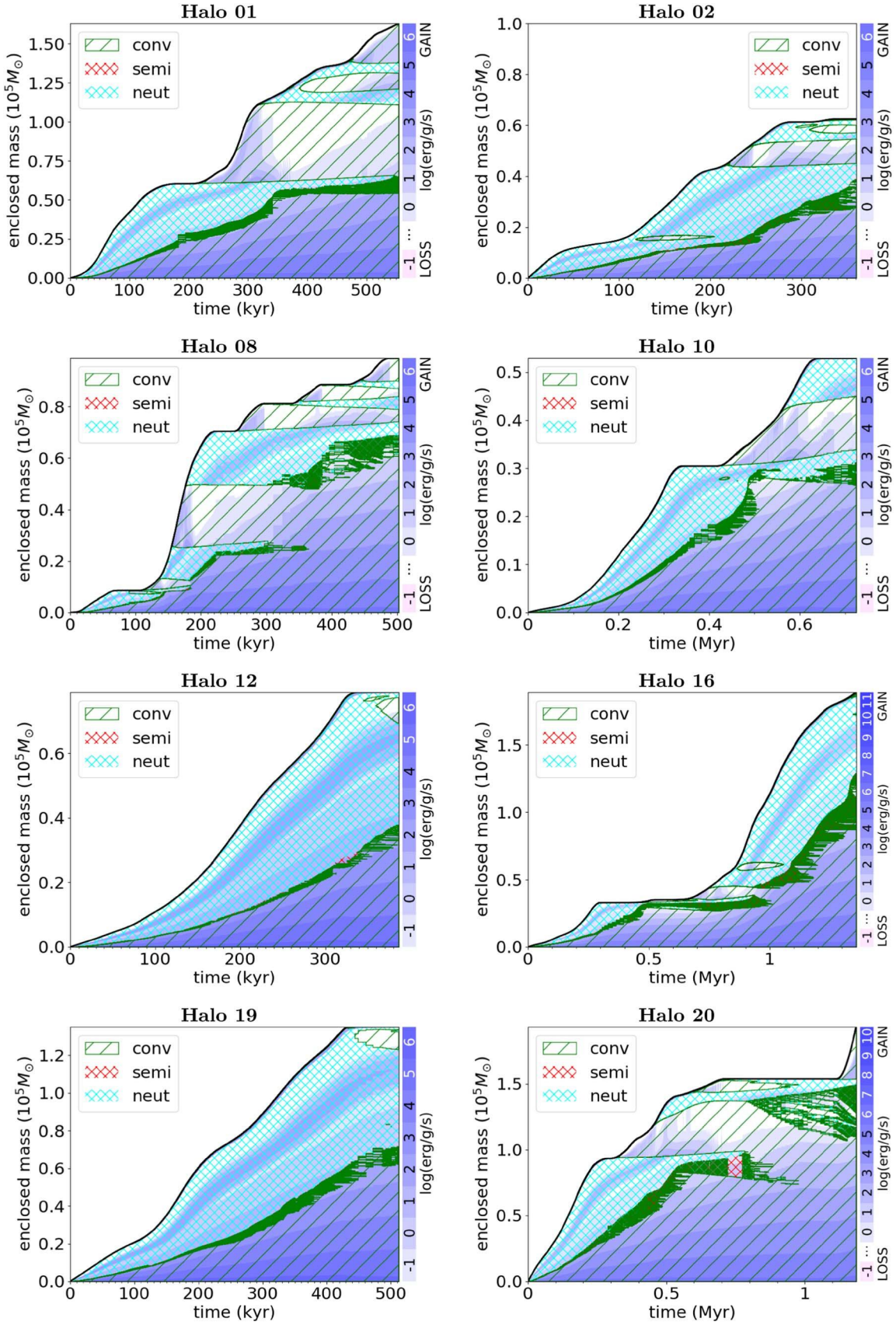

Figure 2. Kippenhahn diagrams of the internal structures of the stars in the satellite disks over time. The blue shades indicate energy generation rates from nuclear burning, green lines denote convective regions, red lines mark semiconvective regions, and light-blue lines indicate radiative/convectively neutral regions.

Table 1
Final State for the Primary and Secondary SMS in Each Halo

Halo	M_1 ($kM_\odot$)	t_{sim} (Myr)	Evol Stage (1)	$X_{c,1}$	M_2 ($kM_\odot$)	t_2 (Myr)	Evol Stage (2)	$X_{c,2}$	Close Pair?
01	134	0.947	MS	0.38	165	0.571	MS	0.40	yes
02	143	1.46	BH[a]	0.34	62	0.378	MS	0.58	yes
08	$\geqslant$186	1.014	BH	⋯	99	0.503	MS	0.56	yes
10	$\geqslant$132	2.006	BH	⋯	53	0.639	MS	0.55	no
12	$\gtrsim$178	1.395	BH	⋯	79	0.380	MS	0.57	yes
16	$\geqslant$109	3.054	BH	⋯	186	1.27	MS (near collapse?)	0.39	no
19	46	1.439	MS	0.28	133	0.426	MS	0.54	yes
20	$\geqslant$178	1.770	BH	⋯	154	1.103	MS (near collapse?)	0.34	no

Note.
[a] Note that the SMS in the primary disk in Halo 02 collapses to a BH during the merger with the secondary disk.

formation of both transient and long-lived convective cells in their otherwise deep, high-entropy radiative envelopes like those in some constant accretion rate models.

In several cases, such as Halos 01 and 16, almost all the mass of the star ends up in its convective core because there is a long ($\gtrsim$100 kyr) quiescent accretion phase (much longer than the Kelvin–Helmholtz timescale) in which the star thermally relaxes and its structure approaches that of an $n = 3$ polytrope (Chandrasekhar 1964; Woods et al. 2020). In this case, the star is likely to become a significant source of ionizing radiation (Sakurai et al. 2015, 2016) as the photospheric temperature rises, tending toward 10^5 K in thermal relaxation (Woods et al. 2020). Critically, this means that even if the SMS in the primary disk is cool and red, stars in nearby disks could be significant sources of ionizing UV feedback in the halo. Understanding the effects of this radiation on the growth of the stars in the halo requires 3D radiation hydrodynamical simulations, but initial studies suggest that it does not prevent them from becoming supermassive (Regan et al. 2020; Latif et al. 2021), in contrast to normal Population III star formation, in which ionizing UV from a few stars in a disk can terminate the growth of the others (Latif et al. 2022a). Our models thus show not only that multiple SMSs form in atomically cooled halos but also that they will be a mix of cool red and hot blue stars. We now consider the evolution of each SMS in the satellite disks in detail.

3.2. Individual Cases

In Halo 01, a secondary disk forms at 400 kyr by breaking off from one of the spiral arms of the primary disk. Throughout its evolution, this companion disk remains in an elliptical orbit around the first with typical separations of 0.5–1 pc. The sharp spike in accretion ∼300 kyr after formation is due to a merger with a clump in the halo. Accretion continues until the second disk merges with the first 650 kyr after formation. At this time, the SMS in the second disk is a somewhat evolved MS star with a central hydrogen fraction of ∼0.4 and a largely convective envelope save for two narrow bands in the outer envelope. The SMS in the first disk is only slightly more evolved, with a central hydrogen fraction of 0.38. Although the subsequent evolution of these stars is beyond the scope of this work, W21 found that the collision of the disks triggered a surge in accretion onto the first star, but the presence of the second SMS may lead to other outcomes. In particular, with a considerable fraction of the secondary disk's mass accumulated in the secondary star, the mass actually available to be accreted onto the primary SMS depends critically on whether the two stars are brought into Roche lobe contact. If so, the deep convective envelope of the (here more massive) "secondary" SMS may favor runaway mass transfer; however, this is beyond the scope of this work, as discussed in Section 4.1.

Halo 02 is an example of a particularly turbulent, chaotic system in which three clumps form and interact with the primary and companion disks (Patrick et al. 2023). Interactions between these clumps and the second disk lead to two large bursts of accretion at 130 and 250 kyr that create an SMS that grows to ∼60 $kM_\odot$ by 275 kyr and has a deep radiative envelope. At this point, there is a brief quiescent phase in accretion due to a close encounter between the two disks. They then merge 378 kyr after the formation of the second disk. The first and second SMSs are 62 and 143 $kM_\odot$, respectively, and have central hydrogen fractions of 0.58 and 0.34, respectively. Notably, the collision of the disks was assumed in W21 to produce a large spike in accretion onto the first SMS that quickly brings it up to the post-Newtonian instability and causes it to collapse. Whether or not this rapid accretion would arise given a detailed treatment of the interaction of these two stars would, however, depend sensitively on whether they are brought into Roche lobe overflow.

Only one satellite disk forms in Halo 08, which lasts from 685 kyr to about 1 Myr after the formation of the first disk. Accretion onto the star is highly variable because of the eccentric orbit of the satellite disk, and the fluctuations correlate with the smallest and largest separations of the two disks, which are ∼0.3 and 2.0 pc, respectively. This accretion history produces the distinctive step-like structure in the Kippenhahn diagram of the star in Figure 2. About 1 Myr after the formation of the primary disk, the star in the second disk has an age of 503 kyr, a mass of 99 $kM_\odot$, and a central hydrogen fraction of 0.56. The SMS in the primary disk, however, has by this time collapsed to a BH, having encountered the post-Newtonian instability at 950 kyr at a mass of 186 $kM_\odot$ and a central hydrogen fraction of 0.38.

The first disk in Halo 10 is stable and does not begin to fragment for 1.14 Myr. The second disk forms ∼1.2 pc from the center of the first in an initially highly elliptical orbit. Two major episodes of accretion drive the growth of the second SMS, in each case building up a deep, high-entropy envelope. Between these episodes there is a long (nearly 100 kyr) quiescent phase during which the star thermally relaxes without becoming entirely convective. It reaches a mass of 53 $kM_\odot$ and a central hydrogen fraction of 0.55 by the end of the simulation. At this time the secondary disk is still in an elliptical orbit

around the first, with separations that vary from 0.5 to 1 pc. The SMS in the first disk, however, has collapsed because of the post-Newtonian instability late on the MS at an age of 1.95 Myr, a final mass of 132 k$M_\odot$, and a central hydrogen fraction of 0.06.

The primary disk in Halo 12 is highly turbulent and frequently fragments, but most of the clumps soon migrate to the center of the disk. The longest-lived of the clumps forms at ∼1 Myr and produces its own disk that survives for 380 kyr. Rapid accretion in this disk creates an SMS with a deep radiative envelope that grows to a mass of 79 k$M_\odot$ with a central hydrogen fraction of 0.57 by the time the two disks merge. About 200 kyr before the destruction of the second disk, the SMS in the primary disk collapsed via the Chandrasekhar instability while still on the MS at a final mass of 178 k$M_\odot$ and central hydrogen fraction of 0.32.

Like Halo 10, Halo 16 has a relatively stable disk that does not fragment for ∼1.5 Myr. A key difference, however, is that the SMS in the primary disk collapses to a BH at about the time the second disk forms because it encounters the post-Newtonian instability at the very end of the MS at a mass of 109 k$M_\odot$, when its core hydrogen is exhausted. It is unclear from the Enzo simulation how X-rays from this BH would affect the evolution of the companion disk, but we discuss some possible outcomes in Section 4.2. As the primary disk continues to fragment, three-body interactions fling the companion disk into a highly elliptical orbit ∼300 kyr after its formation. The initial burst of accretion is followed by a long quiescent phase (∼0.5 Myr) during which the second SMS, which is now ∼40 k$M_\odot$, becomes almost completely thermally relaxed and almost fully convective (Woods et al. 2020). The rapid accretion beginning at ∼750 kyr builds up a massive radiative envelope on top of this convective core, and the mass of the star grows to 186 k$M_\odot$ by the end of the simulation. At this point the SMS is still on the MS in a disk on a long orbit around the first disk, but it appears to be on the verge of collapse. With a mass nearing the upper limit for SMSs with similar accretion rates, the star is unlikely to survive for much longer, so the system may soon produce a DCBH binary.

As the primary disk in Halo 19 begins to fragment, two clumps merge and form a stable companion disk after ∼800 kyr. The initial burst of accretion due to the formation of this disk is particularly strong and builds up a star with a massive convective envelope in ∼500 kyr. Accretion in the disk is so rapid that the evolution of the second SMS overtakes that of the first. By the time the disks merge, the first SMS has reached a mass of 46 k$M_\odot$ and a central hydrogen fraction of 0.28, but the second is at a mass of 133 k$M_\odot$ and a central hydrogen fraction of 0.54. Both stars are still on the MS.

The primary disk in Halo 20 begins to fragment soon after formation and quickly forms a single, massive companion disk. Accretion rates in the disk are fairly high and are rejuvenated at one point when a clump collides with the disk. These high rates quickly build up an SMS with a deep, high-entropy envelope. The companion disk later exchanges mass with the primary disk over a number of orbits, which mostly halts accretion onto the second star and allows it to thermally relax. In the meantime, the SMS in the primary disk collapses at 1.48 Myr to a BH via the post-Newtonian/Chandrasekhar instability late in the MS at a core hydrogen fraction of 0.14 and a mass of 189 k$M_\odot$. At 1.77 Myr, the end of the simulation, the companion disk is in a relatively long elliptical orbit (∼1.8 pc separation) that is growing in radius. At this point, the companion is still on the MS but, as in Halo 16, appears to be about to collapse, having reached a mass of 154 k$M_\odot$.

4. Discussion

In most of the cases above, the accretion history and evolution of the second SMS end with the merger of its host disk with the primary disk. Because the formation of the stars and their trajectories through the halo were not followed in the cosmological simulations, their subsequent evolution cannot be determined here, but we can discuss their expected outcomes.

4.1. MS–MS Pairs

The primary and secondary disks in Halo 01, Halo 19, and nominally Halo 02 merge while their stars are still on the MS. With a maximum physical resolution of 0.014 pc (∼3000 au), the P23 simulations could not determine whether the stars subsequently interacted. Drag forces in the inner disk could bring about a swift merger between them, or they could carve out a gap in the circumbinary disk.

If they interact, their evolution will depend on their mass ratio (Soberman et al. 1997) and their prior accretion histories —in particular, the extent to which they are thermally relaxed. The latter is due to the fact that the response of either star to mass loss, as they come into Roche lobe contact, depends sensitively on the depth and dominant mechanism of energy transport in their outer layers (see, e.g., Ivanova et al. 2013). A deep, radiative envelope with a steep entropy gradient may lose mass without significant changes to the radius of the star. An almost fully convective star will expand in response to mass loss driven by convection flattening the distribution of specific entropy (Woods & Ivanova 2011), leading to further mass transfer and likely ending in a merger.

Such a merger would produce a luminous transient, and any resulting mass loss from these modestly evolved SMSs may imprint unique chemical signatures on their surroundings. For example, Nagele & Umeda (2023) suggested that mass loss from supermassive stellar envelopes could be the origin of the unusual nitrogen abundances in GN-z11 at $z \sim 11$ (Bunker et al. 2023; Cameron et al. 2023) but did not offer a mechanism for such loss. Examples such as Halo 02, wherein one of the SMSs is driven to collapse just as the two accretion disks merge, also show that detailed hydrodynamical calculations (e.g., Glebbeek et al. 2013) are required to properly evolve the structure of the star during enormous surges in accretion (Menon & Heger 2017) but are beyond the scope of our study. If, instead, these supermassive stellar pairs evolve into relatively long-lived binaries, they could later become BH–MS or BH–BH pairs.

4.2. MS–BH Pairs

In Halos 08 and 12 the primary and companion disks merge after the star in the main disk has collapsed to a DCBH, while the SMS in the other disk is still on the MS. The subsequent evolution of both stars and their interactions will depend on the complex dynamics of the innermost, unresolved region of this merged disk. Given that the masses of both the DCBH and the SMS are comparable in both halos, the tidal disruption radius

will be

$$R_t = R_{\rm SMS}\left(\frac{M_{\rm BH}}{M_{\rm SMS}}\right)^{\frac{1}{3}} \sim 10^{12} - 10^{13}{\rm cm}, \quad (6)$$

i.e., of order the supermassive stellar radius. Such a close encounter may arise through Kozai–Lidov interactions with a third body, or through interactions with the surrounding disk. Fragmentation on scales smaller than those resolved here may also lead to the formation of much less massive stars, which could then be torn apart by the DCBH and produce a powerful radio or near-IR transient (Kashiyama & Inayoshi 2016; Regős et al. 2021).

If these objects form a long-lived binary, they will continue to evolve subject to additional torques from the circumbinary disk. Depending on the orbital evolution, the companion SMS may overflow its Roche lobe while still on the MS or as it evolves, in which case its deep radiative envelope could sustain long-lived mass exchange and, perhaps, the formation of a "supermassive" X-ray binary (e.g., Soberman et al. 1997). Eventually, the collapse of the second SMS due to exhaustion of core nuclear fuel or the Chandrasekhar instability will produce a DCBH binary, in which case the subsequent evolution would proceed as discussed below.

4.3. BH–BH Pairs

Some of our models may produce long-period DCBH binaries. At the end of the simulation in Halo 10, the second SMS was still on the MS, but its host disk was in a highly elliptical orbit with the first disk, whose star had collapsed to a DCBH. This long-period orbit suggests that the SMS will collapse to a DCBH before interacting closely with the other BH. Although the secondary SMSs in Halos 16 and 20 are also still on the MS at the end of the simulation, they are both on the verge of collapse via the post-Newtonian instability unless accretion stops. Both of these halos could thus produce long-period ($\sim$1 pc separation) binary DCBHs. The timescale for a merger between the two BHs would depend on their dynamics in the halo and drag forces due to gas flows therein, and the strength of their gravitational wave (GW) signal depends on their masses when they finally do merge. Here we estimate the GW emission from the merger of the DCBH binary in Halo 20 (Robson et al. 2019),[8] considering a sky- and polarization-averaged transfer function and assuming that the orbit has circularized by prior GW emission. The expected signal is shown in Figure 3 for the redshift at which the halo collapses, $z = 17.7$. This merger will be detectable by LISA, as would mergers of the other BH–BH pairs in our halos at their respective redshifts.

5. Conclusions

A growing number of recent numerical simulations indicate that the formation of multiple very massive stars (e.g., Wise et al. 2019; Regan et al. 2020) or SMSs (e.g., Latif et al. 2020; Patrick et al. 2023) was common in primordial, atomic-cooling halos and that these could be the origin of the first quasars in the Universe. Here we have shown that secondary disks in these halos form SMSs whose accretion histories can be coupled to those of the stars in the primary disks via tidal interactions and radiative feedback. Most satellite disks merge with the primary disk in just 1–2 Myr, which could yield supermassive stellar mergers, supermassive X-ray binaries, massive BH seed mergers, and SMS binaries. Such interactions could profoundly affect the evolution of the stars, the SMBH seeds they produce, and their observational signatures, including providing a means for enriching the surrounding environment with material from the SMS envelope. Future simulation efforts should be directed at following the dynamics of these binaries and mass exchange between them using both stellar evolution calculations and hydrodynamical models of their interactions.

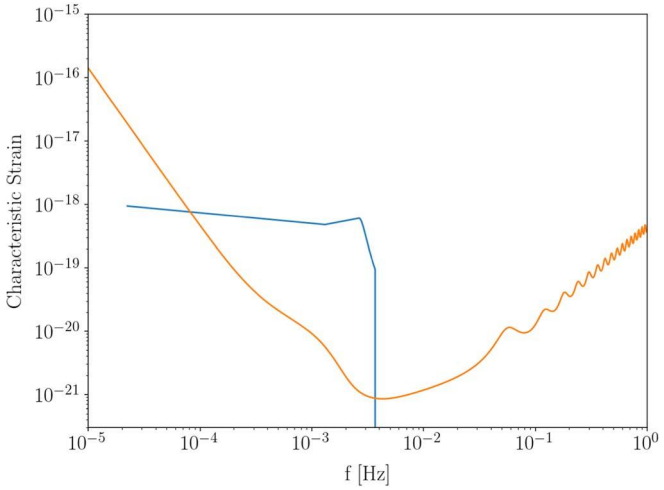

Figure 3. Sky-averaged LISA sensitivity curve (orange) and the observable characteristic strain (blue) from the merger of the DCBHs in Halo 20.

Acknowledgments

T.E.W. acknowledges support from the National Research Council Canada's Plaskett Fellowship. S.P. was supported by STFC grant ST/N504245/1, and D.J.W. was supported by the Ida Pfeiffer Professorship at the Institute of Astrophysics at the University of Vienna. A.H. was supported by the Australian Research Council (ARC) Centre of Excellence (CoE) for Gravitational Wave Discovery (OzGrav) through project No. CE170100004, by the ARC CoE for All Sky Astrophysics in 3 Dimensions (ASTRO 3D) through project No. CE170100013, and by the National Science Foundation under grant No. PHY-1430152 (JINA Center for the Evolution of the Elements, JINA-CEE).

ORCID iDs

Tyrone E. Woods https://orcid.org/0000-0003-1428-5775
Samuel Patrick https://orcid.org/0000-0002-5293-699X
Daniel J. Whalen https://orcid.org/0000-0001-6646-2337
Alexander Heger https://orcid.org/0000-0002-3684-1325

References

Agarwal, B., Khochfar, S., Johnson, J. L., et al. 2012, MNRAS, 425, 2854
Ardaneh, K., Luo, Y., Shlosman, I., et al. 2018, MNRAS, 479, 2277
Bañados, E., Venemans, B. P., Mazzucchelli, C., et al. 2018, Natur, 553, 473
Baraffe, I., Heger, A., & Woosley, S. E. 2001, ApJ, 550, 890
Becerra, F., Greif, T. H., Springel, V., & Hernquist, L. E. 2015, MNRAS, 446, 2380

[8] LISA Sensitivity Calculator available for download from github.com/eXtremeGravityInstitute/LISA_Sensitivity.git.

Becerra, F., Marinacci, F., Bromm, V., & Hernquist, L. E. 2018, MNRAS, 480, 5029
Begelman, M. C. 2010, MNRAS, 402, 673
Bosman, S. E. I. 2021, All $z > 5.7$ quasars currently known, v1.11, Zenodo, doi: 10.5281/zenodo.4610490
Bromm, V., & Loeb, A. 2003, ApJ, 596, 34
Bryan, G. L., Norman, M. L., O'Shea, B. W., et al. 2014, ApJS, 211, 19
Bunker, A. J., Saxena, A., Cameron, A. J., et al. 2023, A&A, 677, A88
Cameron, A. J., Katz, H., Rey, M. P., & Saxena, A. 2023, MNRAS, 523, 3516
Chandrasekhar, S. 1964, ApJ, 140, 417
Chon, S., Hosokawa, T., & Yoshida, N. 2018, MNRAS, 475, 4104
Dijkstra, M., Haiman, Z., Mesinger, A., & Wyithe, J. S. B. 2008, MNRAS, 391, 1961
Fernandez, R., Bryan, G. L., Haiman, Z., & Li, M. 2014, MNRAS, 439, 3798
Glebbeek, E., Gaburov, E., Portegies Zwart, S., & Pols, O. R. 2013, MNRAS, 434, 3497
Haemmerlé, L. 2021, A&A, 647, A83
Haemmerlé, L., Woods, T. E., Klessen, R. S., Heger, A., & Whalen, D. J. 2018a, ApJL, 853, L3
Haemmerlé, L., Woods, T. E., Klessen, R. S., Heger, A., & Whalen, D. J. 2018b, MNRAS, 474, 2757
Herrington, N. P., Whalen, D. J., & Woods, T. E. 2023, MNRAS, 521, 463
Hirano, S., Hosokawa, T., Yoshida, N., et al. 2014, ApJ, 781, 60
Hirano, S., Hosokawa, T., Yoshida, N., & Kuiper, R. 2017, Sci, 357, 1375
Hosokawa, T., Yorke, H. W., Inayoshi, K., Omukai, K., & Yoshida, N. 2013, ApJ, 778, 178
Inayoshi, K., & Haiman, Z. 2014, MNRAS, 445, 1549
Ivanova, N., Justham, S., Chen, X., et al. 2013, A&ARv, 21, 59
Kashiyama, K., & Inayoshi, K. 2016, ApJ, 826, 80
Latif, M. A., Bovino, S., Van Borm, C., et al. 2014, MNRAS, 443, 1979
Latif, M. A., Khochfar, S., Schleicher, D., & Whalen, D. J. 2021, MNRAS, 508, 1756
Latif, M. A., Khochfar, S., & Whalen, D. 2020, ApJL, 892, L4
Latif, M. A., Schleicher, D. R. G., Schmidt, W., & Niemeyer, J. 2013, MNRAS, 430, 588
Latif, M. A., Whalen, D., & Khochfar, S. 2022a, ApJ, 925, 28
Latif, M. A., Whalen, D. J., Khochfar, S., Herrington, N. P., & Woods, T. E. 2022b, Natur, 607, 48
Lodato, G., & Natarajan, P. 2006, MNRAS, 371, 1813
Luo, Y., Ardaneh, K., Shlosman, I., et al. 2018, MNRAS, 476, 3523
Lupi, A., Haiman, Z., & Volonteri, M. 2021, MNRAS, 503, 5046
Maio, U., Borgani, S., Ciardi, B., & Petkova, M. 2019, PASA, 36, e020
Menon, A., & Heger, A. 2017, MNRAS, 469, 4649
Mortlock, D. J., Warren, S. J., Venemans, B. P., et al. 2011, Natur, 474, 616
Nagele, C., & Umeda, H. 2023, ApJL, 949, L16
Nandal, D., Regan, J. A., Woods, T. E., et al. 2023, A&A, 677, A155, arXiv:2306.17223
Patrick, S. J., Whalen, D. J., Latif, M. A., & Elford, J. S. 2023, MNRAS, 522, 3795
Regan, J. A., & Downes, T. P. 2018, MNRAS, 478, 5037
Regan, J. A., & Haehnelt, M. G. 2009, MNRAS, 396, 343
Regan, J. A., Wise, J. H., Woods, T. E., et al. 2020, OJAp, 3, 15
Regős, E., Vinkó, J., & Stermeczky, Z. V. 2021, ApJ, 909, 64
Robson, T., Cornish, N. J., & Liu, C. 2019, CQGra, 36, 105011
Sakurai, Y., Hosokawa, T., Yoshida, N., & Yorke, H. W. 2015, MNRAS, 452, 755
Sakurai, Y., Vorobyov, E. I., Hosokawa, T., et al. 2016, MNRAS, 459, 1137
Schauer, A. T. P., Agarwal, B., Glover, S. C. O., et al. 2017, MNRAS, 467, 2288
Soberman, G. E., Phinney, E. S., & van den Heuvel, E. P. J. 1997, A&A, 327, 620
Suazo, M., Prieto, J., Escala, A., & Schleicher, D. R. G. 2019, ApJ, 885, 127
Tanaka, T. L., & Li, M. 2014, MNRAS, 439, 1092
Tenneti, A., Di Matteo, T., Croft, R., Garcia, T., & Feng, Y. 2018, MNRAS, 474, 597
Timmes, F. X., & Swesty, F. D. 2000, ApJS, 126, 501
Umeda, H., Hosokawa, T., Omukai, K., & Yoshida, N. 2016, ApJL, 830, L34
Valentini, M., Gallerani, S., & Ferrara, A. 2021, MNRAS, 507, 1
Vink, J. S., de Koter, A., & Lamers, H. J. G. L. M. 2001, A&A, 369, 574
Wang, F., Yang, J., Fan, X., et al. 2021, ApJL, 907, L1
Weaver, T. A., Zimmerman, G. B., & Woosley, S. E. 1978, ApJ, 225, 1021
Wise, J. H., Regan, J. A., O'Shea, B. W., et al. 2019, Natur, 566, 85
Wise, J. H., Turk, M. J., & Abel, T. 2008, ApJ, 682, 745
Woods, T. E., Agarwal, B., Bromm, V., et al. 2019, PASA, 36, e027
Woods, T. E., Heger, A., & Haemmerlé, L. 2020, MNRAS, 494, 2236
Woods, T. E., Heger, A., Whalen, D. J., Haemmerlé, L., & Klessen, R. S. 2017, ApJL, 842, L6
Woods, T. E., & Ivanova, N. 2011, ApJL, 739, L48
Woods, T. E., Patrick, S., Elford, J. S., Whalen, D. J., & Heger, A. 2021, ApJ, 915, 110
Woosley, S. E., Heger, A., Cumming, A., et al. 2004, ApJS, 151, 75
Woosley, S. E., Heger, A., & Weaver, T. A. 2002, RvMP, 74, 1015
Wu, X. B., Wang, F., Fan, X., et al. 2015, Natur, 518, 512
Yoshida, N., Abel, T., Hernquist, L., & Sugiyama, N. 2003, ApJ, 592, 645